frontiers | Frontiers in Astronomy and Space Sciences

TYPE Original Research
PUBLISHED 12 July 2023
DOI 10.3389/fspas.2023.1197724

OPEN ACCESS

EDITED BY
Fulvio Franchi,
Botswana International University of Science and Technology, Botswana

REVIEWED BY
Marco Veneranda,
University of Valladolid, Spain
Lucia Marinangeli,
University of Studies G. d'Annunzio Chieti and Pescara, Italy

*CORRESPONDENCE
Marco Ferrari,
marco.ferrari@inaf.it

RECEIVED 31 March 2023
ACCEPTED 08 June 2023
PUBLISHED 12 July 2023

CITATION
Ferrari M, De Angelis S, Frigeri A, Bruschini E, Gómez F and De Sanctis MC (2023), *In situ* measurement and sampling of acidic alteration products at Río Tinto in support of the scientific activity of the Ma_MISS instrument. *Front. Astron. Space Sci.* 10:1197724. doi: 10.3389/fspas.2023.1197724

In situ measurement and sampling of acidic alteration products at Río Tinto in support of the scientific activity of the Ma_MISS instrument

Marco Ferrari[1]*, Simone De Angelis[1], Alessandro Frigeri[1], Enrico Bruschini[1], Felipe Gómez[2] and Maria Cristina De Sanctis[1]

[1]Institute for Space Astrophysics and Planetology-INAF, Rome, Italy, [2]Centro de Astrobiología (CSIC-INTA), Madrid, Spain

We describe the procedures and results of a geological field analysis campaign in the Río Tinto area. This geologically/biologically well-documented site with its rock/water/biology interaction represents an ideal open-air laboratory where to collect spectral data and samples useful for testing space instruments. During the field campaign, we collected a large set of VIS-NIR (0.35–2.5 μm) measurements using the ASD FieldSpec4 portable spectrometer both on biosignature-bearing rocks and on alteration hydrated products (sulfates, clays, oxides, etc.). Furthermore, as a comparison to the data collected in the field, we report the results of the micro-Raman analyses carried out in the laboratory on the collected mineral/rock samples. This work was conducted in the framework of the Mars Multispectral Imager for Subsurface Studies (Ma_MISS) instrument that is a miniaturized visible and near-infrared (VIS-NIR) spectrometer (0.5–2.3 μm) devoted to the Martian subsurface exploration and integrated into the drilling system of the ESA Rosalind Franklin rover mission. Ma_MISS will acquire spectral data on the Martian subsurface from the excavated borehole wall. The scientific results obtained by this campaign confirm that the Río Tinto site is important for enriching the scientific community's grasp on the Martian environment and for obtaining key information on the mineralogical and geochemical evolution of the Martian surface/subsurface. In addition, this work provides crucial preparation for the exploitation and interpretation of the scientific data that the Ma_MISS instrument will supply during the active phase of the mission. This activity is also useful for defining the priorities of the astrobiological objectives on the ground.

KEYWORDS

Martian analogs, VIS-NIR spectroscopy, Río Tinto, Raman, sulfates, clays, Ma_MISS, Rosalind Franklin rover

1 Introduction

1.1 The Río Tinto river: life in extreme conditions

The Río Tinto is a river located in the Iberian Pyritic Belt (IPB) region, a mineralized geological body covering an area of approximately 250 km to a maximum of 60 km in

southwestern Spain (Martin-Izard et a., 2016), formed by hydrothermal activity (Leistel et al., 1997) (Figure 1). The IPB corresponds to an area of Devonian-Carboniferous volcanic and sedimentary rocks containing about 90 deposits of massive polymetallic sulfides that have been mined since the Chalcolithic, i.e., Copper Age, 4500-3000 BC (Leblanc et al., 2000). The Río Tinto originates in Peña de Hierro and flows through the mineral deposits of the IPB (mainly iron and copper sulfide) and reaches the Atlantic Ocean in Huelva, creating the largest acid province in the world. The waters of the Tinto River have a high concentration of ferric iron together with other heavy metals (Cu, Zn, As, Mn, Cr, etc.) kept in solution at an acid pH (average 2.3, Amils et al., 2007) and a high level of microbial diversity, mainly eukaryotic (Aguilera et al., 2006a). Although Río Tinto's acidic waters were once thought to result from environmental damage from mining, research in the area has shown that such an environment predates human activity (Fernández-Remolar, 2003; Amils et al., 2007).

The Tinto River maintains acidic conditions and high iron and other metal ion concentrations along its entire length, despite seasonal climate changes and dilution by tributaries and rainfall. The extreme acidity and high concentration of heavy metals present in the Río Tinto ecosystem are a direct consequence of the biological processes of ferrification and sulfur oxidation of the microbes growing in the rich complex of metal sulfide deposits of the IPB (González-Toril et al., 2003). The microbial and physical characteristics of the river have been suggested as evidence for a subterranean ecosystem sustained by chemolithotrophic anaerobic metabolism of iron and sulfur minerals (Fernández-Remolar et al., 2005; Amils et al., 2007). The important role played by the iron-oxidizing microorganisms is to maintain a high concentration of ferric iron through a mechanism of aerobic respiration: $Fe^{2+} + ½O_2 + 2H^+ \rightarrow Fe^{3+} + H_2O$, which is responsible for maintaining the constant pH of the water thanks to its buffer potential $Fe^{3+} + 3H_2O \rightarrow Fe(OH)_3 + 3H^+$. Microbiological studies identified the prokaryotic phylogenetic belonging of the acidophilic microorganisms of the river. The 80% of the prokaryotic diversity present in the water column corresponds to three bacterial genera: *Leptospirillum* spp., *Acidithiobacillus*, and *Acidiphilium* spp., which are important members of the iron cycle (González-Toril et al., 2003). In addition to the extreme physical and chemical characteristics of the water, Río Tinto exhibits a unique and unexpected degree of eukaryotic diversity in its waters (Amaral Zettler et al., 2002; Aguilera et al., 2006a), and the fact that eukaryotic organisms account for more than 65% of the biomass in the habitat (i.e., the ecological paradox, Aguilera et al., 2013). Members of the phylum *Chlorophyta*, such as *Chlamydomonas*, *Chlorella*, and *Euglena*, are the most frequent species together with two filamentous algae belonging to the genera *Klebsormidium* and *Zygnemopsis* (Aguilera et al., 2006b; Aguilera et al., 2007).

The more acidic part of the river is inhabited by a eukaryotic community dominated by two species belonging to the genera *Dunaliella* and *Cyanidium*, known for their high tolerance to the presence of metals and acids (Visviki and Santikul, 2000). Also, pinnate diatoms (genus *Pinnularia*) are present in the river, which form large brown biofilms. Ifhomycetes are also very abundant in this environment, managing to grow in the extreme conditions of the river. Fungal species such as *Hortaea werneckii* and *Acidomyces acidophilum* have been identified in the Río Tinto with molecular techniques (Amaral Zettler et al., 2002). The mixotrophic community is dominated by microorganisms belonging to the genera *Bodo*, *Ochromonas*, *Labyrinthula*, and *Cercomonas*. The community of consumer protists is characterized by two different species of ciliates (*Oxytrichia* and *Euplotes*). Amoebae belonging to the genera *Valhkampfia* and *Naegleria* are also frequently found in the more acidic parts of the river and a heliozoan species belonging to the genus Actinophyris appears to be the main characteristic predator of the benthic food web of the river. However, not only single-celled eukaryotic systems grow in the extreme conditions of the Tinto River. Several plants grow in acidic riverbank soils demonstrating resistance to heavy metal concentrations in the soils in which they grow, even using the strategy of concentrating metals in their tissues (Rodríguez et al., 2005). This suggests that the management of heavy metals in general and of iron, in particular, is very complex (Schmidt, 2003). Furthermore, these results demonstrate that complex multicellular systems can develop even in extreme conditions, such as those existing in Río Tinto.

1.2 The Río Tinto as a Martian analog site

The selected landing site of the Rosalind Franklin rover mission, Oxia Planum, situated at the Martian dichotomy boundary, is part of a wide basin characterized by the extensive presence of Noachian Fe/Mg-rich phyllosilicates (Mandon et al., 2021; Quantin-Nataf et al., 2021). Hydrated silica and Al-rich phyllosilicates may be present to a lesser extent in the eastern sector of the site (Carter et al., 2016) where Hesperian alluvial and deltaic sediments overlap the Fe-/Mg-rich phyllosilicates. Al-rich clays were also found in the Oxia's catchment area (16.7°N, 337°E), indicating the presence of various clay mineralogies (Turner et al., 2021; Brossier et al., 2022). The deposition of this unit is thought to have occurred either 1) in a subaerial environment with sediments deposited in lacustrine or marine environments); or 2) in a subaerial/surface environment through the deposition of volcanic products or aeolian deposits (Carter et al., 2016; Quantin-Nataf et al., 2021). In the latter case, groundwater alteration or pedogenesis is the most likely scenario for the formation of the Fe/Mg-rich clay minerals observed at the site (Carter et al., 2016). This mineralogical evidence, combined with other morphological features, suggests that Oxia Planum has been affected by long-lasting surface water activity, a factor consistent with conditions favorable for the development of life that make this a Martian site of certain astrobiological interest.

On Mars, obviously, not only the presence of clays testifies the interaction between the pre-existing rocks and the water. In Meridiani Planum or Mawrth Vallis for example, the mineralogy is quite different from that of the Rosalind Franklin rover landing site. The past presence of an aqueous environment is evidenced by the presence of iron-bearing sulfates (Squyres et al., 2004; Farrand et al., 2009). These minerals could result from the breakdown of sulfides (Zolotov and Shock, 2005; Bigham et al., 1996) and testify the presence of a low pH aqueous environment. Similarly, also the detection of hematite at a regional scale (Christensen et al., 2001) could indicate that pre-existing rocks have undergone chemical erosion in aqueous conditions (Rieder et al., 2004; Squyres et al., 2004). Iron oxides associated with sulfates are the characteristic minerals that form in modern sediments and young terraces of

FIGURE 1
View of the Río Tinto river in Berrocal.

the Río Tinto: they are hydrojarosite, schwertmannite, copiapite, coquimbite, natrojarosite, gypsum, and other sulfate minerals. Goethite and hematite are the predominant minerals in the ancient terraces of the Tinto basin (Fernández-Remolar et al., 2005).

From these studies, it emerges that some mineralogies detected in the Río Tinto are consistent with those detected in various parts of the Mars surface but could seem far from the mineralogies detected in Oxia Planum. In this case, the non-detection of sulfates and iron-bearing oxides could be linked to the low spatial resolution of the instruments that operated in remote sensing. *In situ* investigations that will be carried out at the Rover Rosalind Franklin scale and in particular the acquisitions made by Ma_MISS (with a spatial resolution of 120 μm) could reveal the presence of sulfate veins such as those revealed in Gale Crater by the ChemCam instrument (Nachon et al., 2014). A further indication supporting the identification of minerals that form in acid conditions could be supported by the lack of detection of carbonates in Oxia Planum. Analogies between Oxia Planum and Río Tinto can be represented by the aqueous alteration processes that formed clays. On the other hand, differences in the resulting clay assemblage could be due to the different environmental conditions (e.g., pH, temperature, etc.) as shown by laboratory experiments (Krzesinska et al., 2020).

Since the presence of iron-bearing minerals detected at the Río Tinto is not only due to the acid drainage of exposed minerals but, on the contrary, can be attributed to the role of bacteria that play a key role in making this place an extreme environment, the Río Tinto represents a peculiar site from an astrobiological point of view where to collect and measure samples useful for the scientific data interpretation.

The Río Tinto analog site is currently used by international research centers and industry (e.g., Wood Hole Oceanographic Institute, NASA Ames Research Center, University of Washington at St. Louis, Honey Bee Robotics) and is among analog sites that Europlanet Transnational Access (TA) programme supports, promoting the visit the field sites for European and international researchers (e.g., Europlanet TA1 facility 2).

In this terrestrial analog site, we performed a VIS-NIR measurement campaign intending to detect Martian analog compositions and testing acquisition procedures in support of the Ma_MISS instrument scientific activity.

1.3 The Rosalind Franklin rover mission

The Rosalind Franklin rover mission will be launched in 2028 to determine whether life ever existed or is still active on Mars and characterize the water/geochemical environment as a function of depth in the shallow subsurface. The rover payload (i.e., Pasteur payload) consists of panoramic instruments, contact instruments, the Analytical Laboratory Drawer (ALD), and two subsystems (Vago et al., 2017). Among the panoramic instruments, there are: 1) The Panoramic Camera (PanCam) composed of two wide-angle stereo cameras (WAC) and one high-resolution camera (HRC) to investigate the landing site environment and geology, it will be used to image collected samples (Coates et al., 2017); 2) a context Infrared Spectrometer that will substitute the Russian one ISEM (Korablev et al., 2017) capable of detecting the infrared spectrum of a given target and determining its composition; 3) the radar-GPR WISDOM with surface penetration for shallow depths, capable of detecting the presence of water, ice, and stratification down to depths of 3 m, with a vertical resolution of a few centimeters (Ciarletti et al., 2017); and 4) ADRON a gamma rays and neutrons detector that will investigate the number of thermal and epithermal neutrons scattered (with a range from 0.01 eV to ~100 keV) in the subsurface, to determine the possible presence of ice, hydrated minerals, and hygroscopic and/or capillary water (Mitrofanov et al., 2017).

Among the contact instruments, there is 1) the CLose-UP Imager (CLUPI) which is devoted to investigating rock targets, and cuttings produced during drilling operations, and imaging the

collected samples with sub-millimeter resolution (Josset et al., 2017), and Ma_MISS (Mars Multispectral Imager for Subsurface Studies; De Sanctis et al., 2017; De Sanctis et al., 2022), the miniaturized visible and near-infrared (VIS-NIR) spectrometer (0.5–2.3 μm; spatial resolution 120 μm; spectral resolution ~20 nm) integrated into the drilling system devoted to Martian subsurface exploration. The spectral data collected by Ma_MISS on unexposed rocks will be crucial for 1) the determination of the composition of the subsurface rocks, 2) the optical and physical properties of materials (i.e., grain size), and 3) the reconstruction of a stratigraphic column, getting clues about subsurface geological processes. In addition, the Ma_MISS data could give some hints about the presence of biomarkers in the subsurface because the presence of organic matter can affect some spectral parameters (Ferrari et al., 2023). Ma_MISS will run periodically during pauses of the drilling activity and depending on the adopted scientific strategies, it will perform "columnar" or "ring" acquisitions using the vertical translation or the rotation of the drill reconstructing the hyperspectral image of the drill's borehole (De Sanctis et al., 2017).

The ALD contains the instruments devoted to the analysis of the collected samples, these are: 1) MircOmega a NIR hyperspectral camera for characterizing mineralogy and organics at the micrometric scale (Bibring et al., 2017); 2) the Raman Laser Spectrometer (RLS) that provides information both on the mineralogy and to establish the presence of organic and inorganic carbon (Rull et al., 2017) and 3) the Mars Organic Molecule Analyzer (MOMA) that can identify a wide range of organic molecules, even if they have a low concentration (Goesmann et al., 2017).

The two subsystems onboard the Rosalind Franklin rover are the Drill capable of obtaining samples up to 2 m depth and the Sample Preparation and Distribution System (SPDS) which manage the collected samples and delivers them to the analytical laboratory instruments (Vago et al., 2017).

In this framework, we performed a field campaign in the Río Tinto area where we performed a set of VIS-NIR measurements using the portable spectrometer ASD FieldSpec4 both on acidic alteration minerals and on biosignature-bearing geological samples.

In addition, for each analyzed mineral/rock on-field, we collected representative samples that we measured by micro-Raman spectroscopy at the INAF-IAPS laboratories (Rome, Italy). This work will provide crucial preparation for the exploitation and interpretation of the scientific data that the Ma_MISS instrument will acquire during the active phase of the next Mars mission.

2 On-field activity and laboratory measurements

During the field campaign, we visited six different locations (Figure 2) performing an extensive series of VIS-NIR measurements using our portable spectrometer on rocks containing biosignatures and on acid alteration products. The instrument we used is described in De Angelis et al. (2014), consisting of the ASD FieldSpec4 spectrometer, having a detection spectral range of 0.35–2.5 μm. This range is covered by three separate detectors: the VIS (0.35–1.0 μm),

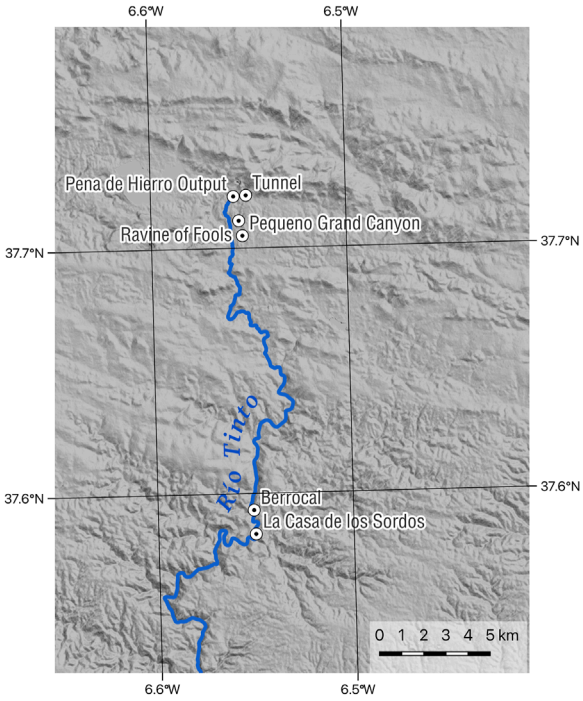

FIGURE 2
Locations visited during the field campaign in the Río Tinto area.

the SWIR1 (1.0–1.8 μm), and the SWIR2 (1.8–2.5 μm). Thus, the entire VNIR spectrum is obtained by joining the spectra detected in each spectral sub-region. The spectral resolution is in the range of 3–8 nm and a spatial acquisition spot ranges from 2 to 3 mm (depending on the measurement distance that in this case ranges from 0.5 to 1 cm). An optical fibers bundle was used to collect the reflected light. We collected several reflectance spectra for each selected lithotype using sunlight as a light source and a 99% Spectralon target as a reference in the VIS-NIR range.

The differences between the setup used in the field (ASD FieldSpec4) and Ma_MISS in terms of spectral range and resolution are not relevant in this work phase. On the other hand, these differences will be considered when the Río Tinto samples will be measured using the Ma_MISS laboratory model.

In addition, for each mineral/rock measured, we took a representative sample to be used for laboratory measurements (Table 1). The amount of the collected samples is variable depending on the nature of the sample itself.

For each collected sample, we recorded the following data at the time of collection: one picture of the context, one picture of the sample with the reference scale, the three-dimensional orientation of the sample, and the geographic coordinates at the collection point using WGS84 reference system, recording the accuracy of the fix at the sample station. Every sample was sealed in a specific container to avoid any contamination. The samples' metadata were registered in the System for Earth Samples Registration (SESAR) for long-term archival. Every sample received a unique IGSN code (igsn.org) for referencing in this project, but also in future ones.

TABLE 1 Summary table reporting for each visited location, the number of the acquired VIS-NIR measurement spots, and the collected samples.

Locations	Measurements	Collected samples
Ravine of fools	77	8
Pequeño Grand Canyon	19	12
Berrocal	27	14
La Casa de los Sordos	12	2
Tunnel (Río Tinto birth)	62	8
Peña de Hierro	—	2
Total	197	46

The collected samples were analyzed with the Bruker SENTERRA II Raman micro-spectrometer at the C-Lab at INAF-IAPS in Rome. This setup has a dual-wavelength excitation laser source (785 and 532 nm) and is equipped with a computer-controlled sample stage with a minimum step width of 50 nm and accuracy of 1 μm that allows fully automated mapping and imaging measurements. The micro-Raman setup is equipped with long working distance objectives (e.g., Olympus 50x LWD; WD: 10.6 mm). The micro-Raman characterization of the collected samples was performed in support of the VIS-NIR measurements collected on the field. The Raman complementary mineralogical identification will be used to understand spectral shapes that often characterize clays and salts spectra in the VIS-NIR range. This technique was usually used combined with VIS-NIR spectroscopy (Hughes et al., 2023) In addition, the Raman micro-spectroscopy was used to characterize at the small scale the relationship between minerals and organics because Raman represents an effective tool for constraining the nature of organic molecules like chlorophyll and carotenoids.

3 Results

Here we report one case study for five of the six visited locations: Ravine of Fools, Pequeño Grand Canyon, Berrocal, La Casa de los Sordos, and the Tunnel except for Peña de Hierro where VIS-NIR measurements were not collected in the field (viz. Table 1). The micro-Raman laboratory data were collected on all the samples measured on the field with the VIS-NIR portable spectrometer. Some samples collected during this field campaign will be measured with the Ma_MISS laboratory breadboard (De Angelis et al., 2022; Rossi et al., 2022) and the data we will compare with those acquired in the field and the result will be the object of a following publication.

3.1 Ravine of fools: simulation of a Ma_MISS columnar acquisition across a fluvial terrace stratigraphy

The "Ravine of the fools" (37°42′30.6″N 6°33′29.4″W) is located along a freshwater stream (Figure 3A) that carves a valley immediately north of a deposit of mining tailing deposit, which we will here refer to as the Pequeño Grand Canyon. Along this valley, the stream activity has generated fluvial terraces where the stratigraphy is exposed. These river terraces represent *ad hoc* sites where it is possible to collect a series of spectra across the stratification (Figure 3B). This type of on-field acquisition results useful to simulate a Ma_MISS columnar acquisition in the Martian subsurface. Figure 3B shows an exposed wall of a fluvial terrace situated on the orographic left of the stream. The blue dots represent the 37 acquisition points of the VIS-NIR spectrometer. The distance $(\Delta)_z$ between each acquisition point is about 1 cm. The total length of this survey is about 38 cm. It crosses six different lithotypes, almost all of which appear in horizontal stratification (A, B, C, D, E) except for type F, which represents a black spot embedded in the stratification. This acquisition was made going from the top (layer A) to the bottom (layer E) including the F black spot. All the collected spectra are reported in Figure 3C, the large noise near 1,400 and 1,900 nm is due to the atmospheric water that is difficult to compensate with the reference target measurement using the sunlight as a light source during open-air acquisitions.

In Figure 4A the full-range average spectra of each lithotype are reported. Layers A, C, and E show spectra with similar characteristics especially in the visible range and near 900 nm related to Charge Transfer Absorption (CTA) and Crystal Field Absorption (CFA) effects as highlighted by the gray and orange bands respectively in Figure 4B. In contrast, layers B and D do not show these strong bands at the same locations and D shows a high level of reflectance in the visible range. Layer F shows a lower reflectance level with a strong red slope in the NIR range; Figure 4C shows that also in the NIR field the layers A, C, and E are like each other showing a band close to 2,200 nm which in the case of E is wider than the others. In addition to this band, the D layer shows absorption at 2,265 nm which is also present in the B layer spectra although it appears to be a weaker absorption. The D layer in addition to this band shows a doublet with band centers at 2,165 and 2,210 nm and a band near 2,285. The black spot (F) shows no absorption at the same wavelength as the other lithotypes but appears to have a very broad absorption centered near 2,230 nm.

3.2 Pequeño Grand Canyon: simulation of a Ma_MISS columnar acquisition in a mine tailings basin

The Pequeño Grand Canyon (37°42′09.5″N 6°33′10.1″W) is a large mining tailings basin where surface waters flowing into the Río Tinto have carved a small canyon. This deposit appears fine-grained and intensely layered with a random succession of two different lithotypes. The grey layers have a very fine grain size and plastic behavior, whereas the white ones have a larger grain size and sandy texture. The thickness of grey and white layers is comparable and ranges from a few millimeters to a few centimeters with sub-horizontal bedding throughout the entire area. Figure 5A shows the south sector of the Pequeño Grand Canyon where we performed the spectroscopic survey across the stratigraphy; Figure 5B shows the exposed wall of the mining waste deposit where, in this case, we collected 11 acquisition points with variable spacing $(\Delta)_z$ collecting one spectrum per layer for a total length of the survey of about

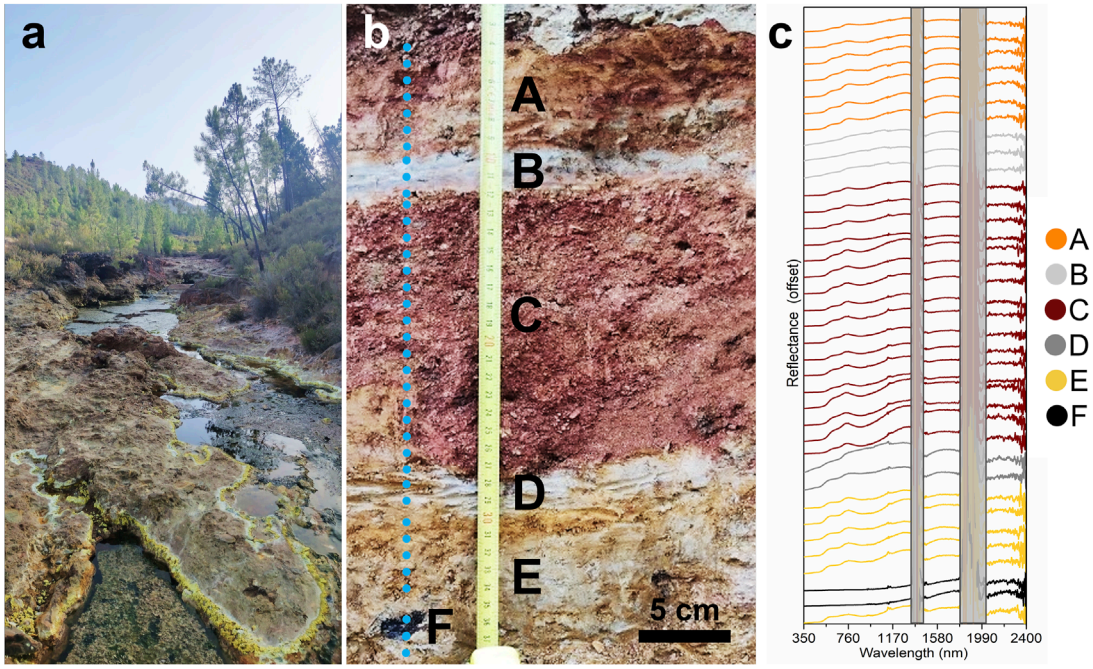

FIGURE 3
The Ravine of fools: **(A)** the freshwater stream and yellow efflorescences at the shoreline are iron-bearing sulfates; **(B)** the exposed wall of the fluvial terrace, letters indicate the six different lithotypes and the blue spots the positions of all the collected spectral measurements; **(C)** All the 37 acquired spectra stacked in the order of acquisitions, the colors indicate the different lithotypes. The grey bands cover high noise spectral range parts due to a bad compensation of the atmospheric water.

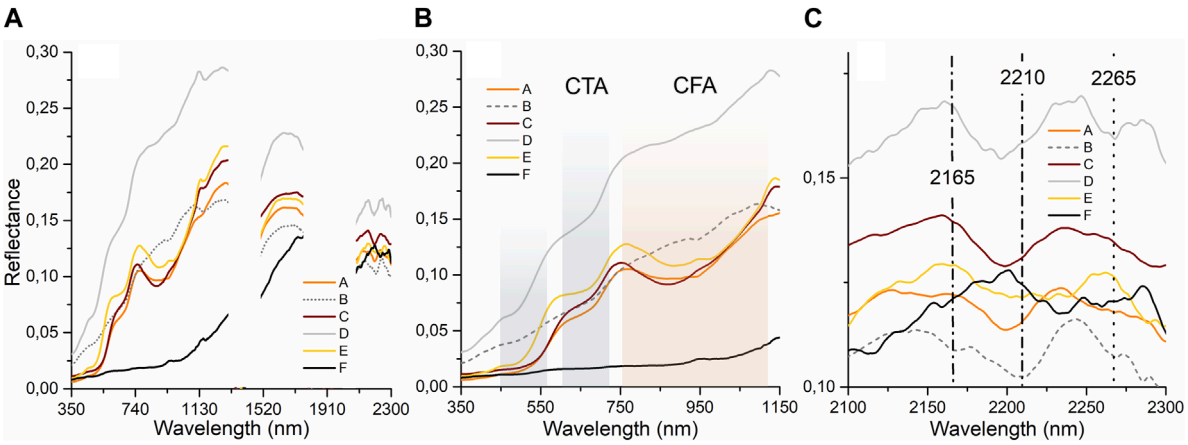

FIGURE 4
(A) VIS-NIR average spectra of every single lithotype; **(B)** collected spectra in the range 350–1,150 nm, the grey and the orange bands highlight the Charge Transfer Absorption (CTA) and the Crystal Field Absorption (CFA) respectively, the gaps in the spectra are due to the removal of spectral ranges that are affected by large noise; **(C)** 2,100–2,300 nm range, the vertical lines mark the position of the absorption of the layers B and D.

15 cm crossing the stratigraphy. This acquisition was made going from the top (white layer) to the bottom (grey layer). All the collected spectra are reported in Figure 5C, the large noise near 1,400 and 1,900 nm is due to a bad compensation of the atmospheric water.

Figure 6A shows the average spectra of the gray and white layers as the result of the spectral diversity found in the Pequeño Grand Canyon. The average spectrum of the gray layers shows a 430 nm band and a lower reflectance level than that of the white layers. In contrast, the average spectrum of the white layers has a higher reflectance level and shows no absorption band in the visible range. Figure 6B shows the same spectra after continuum subtraction. This operation on the spectra allows us to highlight the differences in the depth of some absorption bands

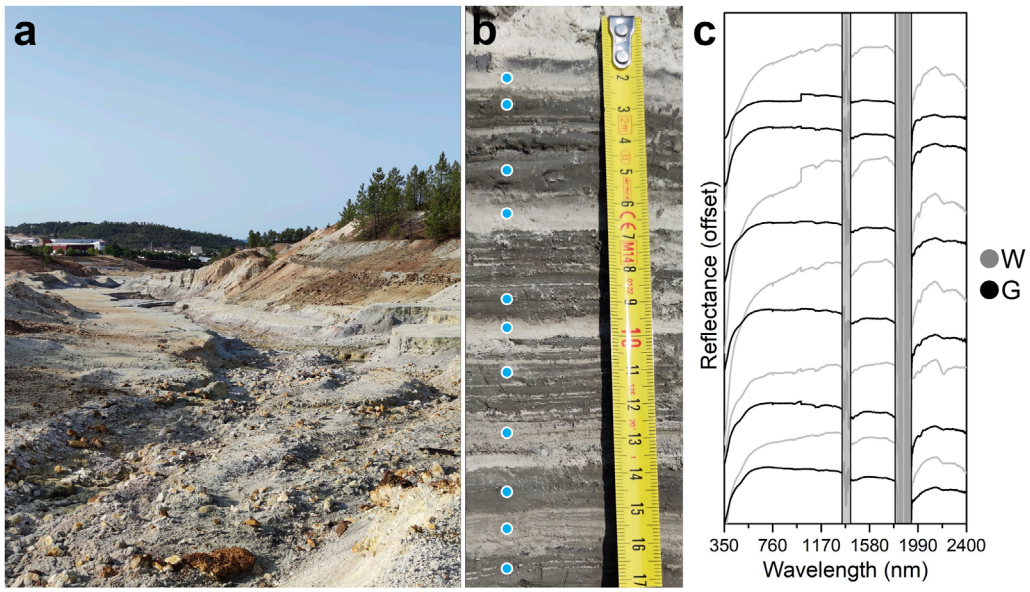

FIGURE 5
The Pequeño Grand Canyon: **(A)** The mining waste dump carved by surface water flow; **(B)** the exposed wall of the small canyon showing layering, the blue spots report the positions of the eleven collected measurement spots; **(C)** All the 11 acquired spectra stacked in the order of acquisitions, the black spectra are referred to grey (G in the caption) layers and the grey spectra to the white layers (W in the caption). The feature near 965 nm in some spectra is an artifact due to the junction of different instrument detectors' spectral ranges. The grey bands cover high noise spectral range parts due to a bad compensation of the atmospheric water.

common to the two different layers. Both layers show bands near 1,400 and 1,900 nm, which in the case of the gray layers are stronger. The continuum removal procedure normalizes reflectance spectra to facilitate the evaluation of individual absorption features from a common baseline. We subtracted a baseline from each spectrum. The baseline was drawn using straight-line segments that connect local spectra maxima individually for each spectrum by selecting anchor points in the intervals where no absorption features were observed. Figure 6B also highlights a difference in terms of the depth of the band at 2,206 nm, which in the case of the representative spectrum of the white layer is considerably deeper.

3.3 Berrocal: collecting acidic alteration features on volcanic rocks

Berrocal is located about 10 km south of the town of Nerva (37°35′35.1″N 6°33′03.5″W). In this location, on the riverbed, there are pebbles partially rounded by the fluvial activity that are visibly altered by the acidic environment (Figure 7A), with surface colorations tending to reddish and with grey/beige alteration features along fractures and pebble boundaries (Figure 7B). These pebbles, probably consisting of a volcanic rock, appear to be cemented to the ground by salty crusts that make the substrate a kind of conglomerate consisting of these centimetric pebbles with a fine-grained matrix. At this location, we decide to collect data from a fragment of these rock pebbles cemented to the ground to evaluate by VIS-NIR spectroscopy both the composition of the rock, trying to derive information on metamorphic minerals related to hydrothermal processes (Large et al., 2001), and the late alteration related to the effect of the acidic environment resulting from exposure to the acidic river water.

The location of the analyzed spots on the pebble and the resulting spectra are reported in Figures 7C, D respectively. The spectrum of the un-altered rock (green spectrum in Figure 7D) is characterized by a broad absorption centered at 1,065 nm with a left shoulder at 750 nm. A smaller absorption band is located at 660 nm. Another weak but resolvable absorption is centered at about 400 nm. In the NIR range the spectrum is characterized by a V-shaped absorption with a center at ~1,550 nm. The most prominent feature of the spectrum is a doublet with band centers at 2,257 and 2,350 nm. The other three spectra resulting from acidic aqueous alteration show spectral features completely different from the unaltered surface. The spectrum collected in correspondence with the blue spot (blue spectrum in Figure 7D) is characterized by a deep absorption band at 930 nm with a left shoulder at 775 nm. Smaller absorption features are found at 680 and 500 nm. In the NIR range it is possible to see an inflection at 1,900 nm and very weak features at 2,257 and 2,350 nm which are the same absorption bands observed in the un-altered rock spectrum (green in Figure 7D) but almost completely obliterated by the alteration process. Spectrum collected in the red spot position, (red spectrum in Figure 7C), the main absorption is found at 905 nm. It is characterized by a strong intensity and a marked asymmetry. In the visible region, the only other observable absorption band is located at 435 nm. The NIR region is characterized by weak absorptions superimposed to high noise regions, so it is not easy to assess their shape and position. There is a small absorption feature at 2,265 nm.

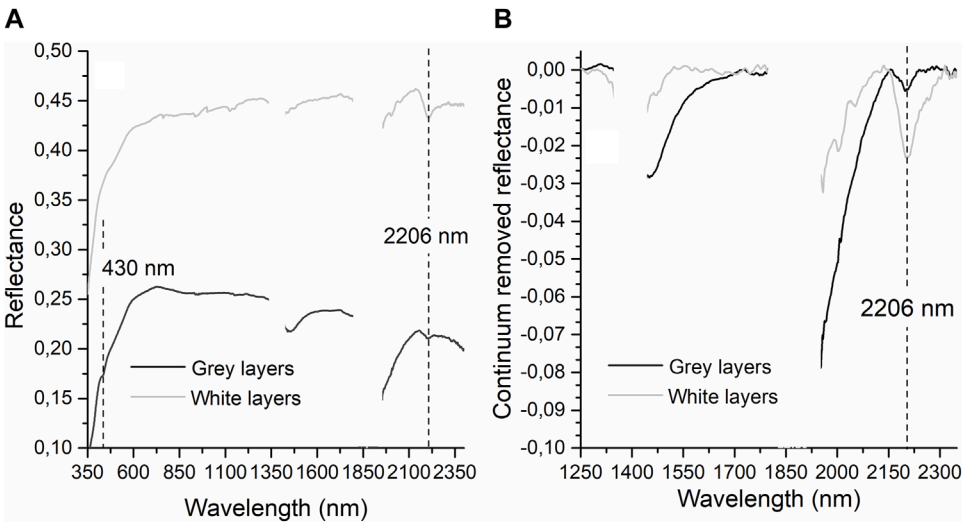

FIGURE 6
(A) VIS-NIR average spectra of the grey and white layers; **(B)** Continuum removed spectra in the range 1,250–2,350 nm. The data near 1,400 and 1,900 nm were removed for high noise due to bad compensation of atmospheric water. The gaps in the spectra are due to the removal of spectral ranges that are affected by large noise.

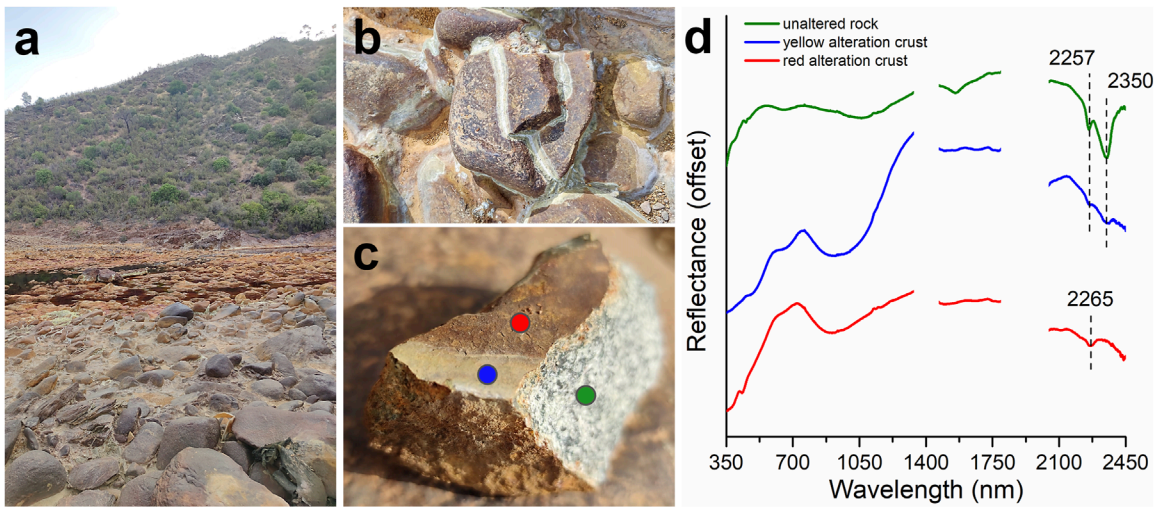

FIGURE 7
Berrocal: **(A)** Rock pebbles on the Río Tinto riverbed; **(B)** Altered pebbles cemented on the riverbed showing alteration features on the surfaces; **(C)** Sample of metamorphosed volcanic rock with reporting the colored spots of the on-field spectral measurements; **(D)** Spectra collected in the range 350–2450 nm on different samples parts showing different alteration features along with the "fresh" mineral assemblage (green spot). The spectra are offset for clarity and the gaps in the data are due to the removal of spectral ranges that are affected by large noise.

3.4 La Casa de los Sordos: collecting acidic alteration features on river sediments

This site is located This location is along the course of the Río Tinto (37°35′00.6″N 6°33′00.5″W) at just under a kilometer downstream from the location described in the previous section (3.3 Berrocal). The spot where we made the VIS-NIR measurements and collected the samples is in correspondence with the inlet of a freshwater tributary into the Río Tinto. The fluvial sediments that characterize the location appear stratified with grain size and color varying from yellow to gray and with a preponderance of purple sediments (Figure 8A). In this case, we chose to characterize the purple sediments that at their base have a slightly less sorted grain size layer consisting of a very fine light gray part along with grains of different nature of higher in size (i.e., the left side of the sample in Figure 8B).

In the case of the sample characterized by a purple color collected in the site "La Casa de Los Sordos," the spectra are characterized by well-defined electronic absorption in the visible spectral range. The spectrum collected in the bottom grey layer

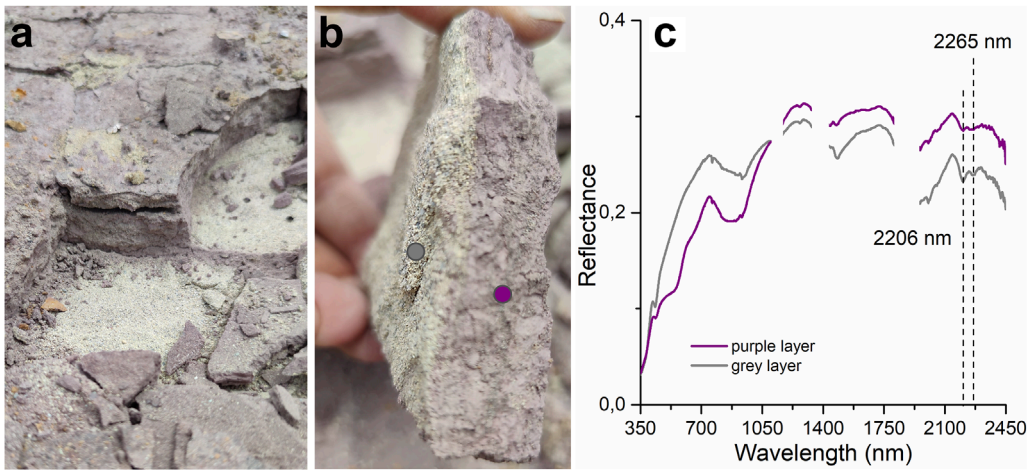

FIGURE 8
La Casa de Los Sordos: **(A)** Context picture of the sampling point; **(B)** Purple sample with a grey layer on the base (left side), the grey and the purple spots report the positions of the collected measurement"; **(C)** Spectra collected in the range 350–2,450 nm the two different samples parts both showing bands at 2,206 and 2,265 with different depth, the gaps in the spectra are due to the removal of spectral ranges that are affected by large noise.

has slightly different spectral features with respect to the purple top layer. In all the spectra we see a strong absorption centered at near 880 nm with a left shoulder near 775 nm. In the bottom layer, this band has a center at higher wavelengths (935 nm). Other well-defined absorptions occur near 550 nm and 440 nm for the top layer while the bottom layer does not show the band near 550 nm (Figure 8C). The NIR region of the spectrum is characterized by several absorption bands. Unfortunately, the absorption occurring around 1,400 nm and 1,800–1,950 nm are superimposed to the high noise region of the on-site spectra due to a bad compensation for the atmospheric water. Despite the presence of a noisy signal in the on-site spectra, it is possible to see a clear inflection roughly centered near 1,400 nm, another complex absorption around 1,900 nm features, and a doublet at 2,205 and 2,265 nm.

3.5 The tunnel: Searching for biosignatures

The tunnel (Figure 9A) is located near the Río Tinto birth (37°43′17.1″N 6°33′03.9″W) and is a structure above which is the road to Peña de Hierro and below which flows the Río Tinto, which in this site, has the appearance of a stream. Previous studies that characterized the ecosystem of this site (Gómez et al., 2012) highlight its astrobiological relevance. The tunnel is a man-made artifact probably made for logistic purposes useful to mining extraction and was built using rocks that have mineralogical characteristics entirely akin to those of the mining area. Internally, the tunnel has walls covered with saline/mineral inflorescence due to the percolation of meteoric water through the embarkment that contains the tunnel itself. The water percolating through the rocks alters/oxidizes the metal-rich minerals (i.e., polymetallic sulfides) and deposits salts at the interface between the tunnel wall and the open air. The inner walls of the tunnel, where not covered by saline inflorescence seem to be made of rock blocks with characteristics entirely like those of the surrounding area held together by cement mortar. Figure 9B shows a detail of the left wall (referring to the left riverbank) covered with saline efflorescences of different colors. There are orange and white efflorescences forming a surface below which is possible to find a green patina due to the presence of alleged organic material. On these three different material types, we collected VIS-NIR spectra, the measured points are indicated by the circles in Figure 9B with the colors corresponding to the related spectra shown in Figure 7C. In this case, we show the spectra only in the range 400–700 nm since the poor illumination conditions inside the tunnel caused a high noise in the NIR range. The spectrum collected on the orange efflorescences (orange spectrum in Figure 9C) shows strong absorption in the region of 400–500 nm and near 850 nm. The spectrum collected on the white efflorescence (grey spectrum in Figure 9C) shows a higher level of reflectance and an absorption band near 430 nm and a shallower absorption at around 500 nm with respect to the orange one. The spectrum collected on the green patina (green spectrum in Figure 9C) shows a different spectral shape to the previous ones with absorption bands near 430, 620, and 675 nm, with a scattering peak in the green region at 532 nm and one at 650 nm. In the case of the spectra collected on the green material, the absorption band close to 430 nm could be consistent with the presence of spots of white material, which are not discernable among the green patina at the spatial resolution of the ASD FieldSpec4. This issue could be fixed by calculating the band centers in the region of 430 nm on both white and green spectra (Figure 11).

In a different part of the left wall of the tunnel, the efflorescences are thicker and appear to be tougher with respect to those previously analyzed. By collecting a sample of this type, we detached a thick mineral crust (Figure 10A) incorporating in the mineral matrix a 2-mm-thick, green-colored layer immediately below the yellowish surface. Internally, where the green layer is not present, the mineral crust appears white, while on the side where it was attached to the wall (wall side, left side of the sample, Figure 10A) it has a reddish color. Once collected, the sample was taken out of the tunnel to have the maximum possible solar illumination, useful for collecting the

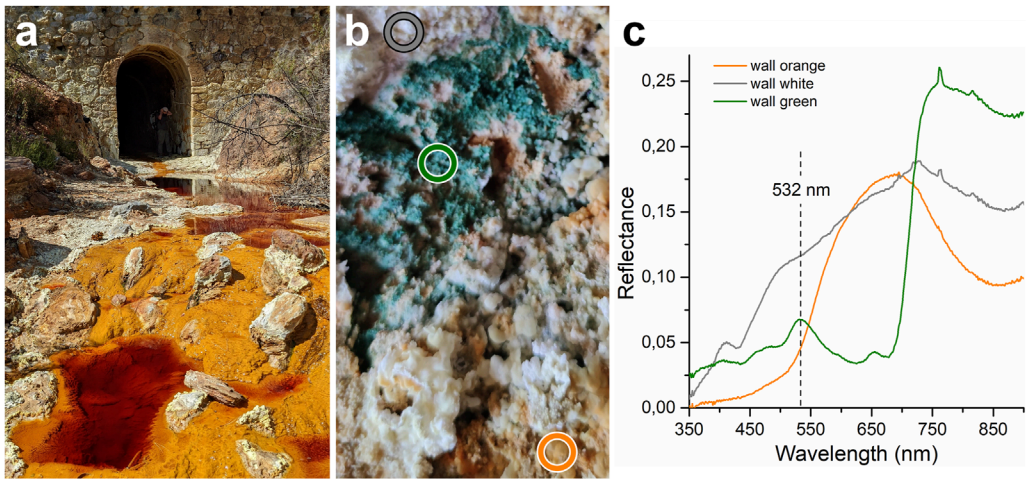

FIGURE 9
The tunnel: **(A)** The Río Tinto River flowing under the tunnel; **(B)** Part of the left wall of the tunnel where there are white and orange efflorescences, below which there is a green patina, the colored circles report the positions of the collected measurement; **(C)** Spectra collected in the range 350–900 nm on the two different efflorescences and on the green patina.

spectrum over the entire Fieldscpec4 range. The spectra collected on the reddish side, in the inner white part of the mineral crust, and on the green layer are shown in Figure 10B. The white crust spectrum shows a higher reflectance than the other two spectra and shows an absorption band near 430 nm and three strong absorption bands near 1,195, 1,450, and 1,750 nm in addition to a shallower absorption near 985 nm. The spectra collected on the green layer, in the visible part of the range (Figure 10C), show the same spectral characteristics as that collected on the green patina on the tunnel wall (Figure 9C) but at higher wavelengths it shows the same spectral shape and absorptions as that of white crust. In particular, the spectra collected on the white mineral crust and that on the green layer show absorption with two minima in the band at 1,195 nm and three minima in the band near 1,750 nm. The spectrum collected on the reddish layer has a very different spectral shape from the other two. It has a lower level of reflectance and strong absorptions near 400, 650, and 950 nm. This spectrum also shows an absorption feature near 1,440 nm but unlike the other two, this band does not show three distinct minima.

To better understand whether there is an actual difference in the position of the bands near 430 nm in the spectra of the green layer and that of the white crust we present data collected on the tunnel wall (Figure 11A) and those of the mineral crust sample (Figure 11B) after the spectra continuum removal. Also in this case we subtracted a straight-line segment baseline from each spectrum. This procedure allows a more accurate assessment of the band positions, however, mixing effects between the two components of the spectrum (white layer and green patina) due to the spatial resolution of the ASD FieldSpec4 could be present. In both cases, data collected on the tunnel wall show the band centers at 435 nm in the case of the white material and at 439 nm in the case of the green ones. This determination will be useful in the characterization of the organic material that grows below the white mineral crust surface.

3.6 Laboratory micro-Raman analysis

To better characterize the mineralogy and the nature of organics, the types of material measured with the VIS-NIR spectroscopy in the field were measured in the laboratory with the micro-Raman spectrometer. Figure 12 shows the Raman spectra collected on the two types of efflorescences on the wall and described in Section 3.5. In the case of the orange efflorescence (Figure 12A), Raman peaks were detected at 271, 303, 474, 607, 990, 1,020, and 1,107 cm^{-1}. The case of the white efflorescence sample shows peaks at 208, 282, 501, 598, 1,023, 1,096, and 1,198 cm^{-1}. The Raman data confirms a clear mineralogical difference between the two types of efflorescence that characterize the tunnel wall confirming the spectral diversity found in the VIS-NIR data.

The sample collected inside the tunnel (i.e., the sample in Figure 10A) in the white parts shows a crystal structure consisting exclusively of colorless tabular crystals but also prismatic crystals that have dimensions in the range of 50–300 microns (Figure 13A). In correspondence with the green layer, the colorless crystals coexist with green-colored material consisting of spheroidal elements with dimensions of about five microns. The Raman spectrum collected in this area of the sample and shown in Figure 13B shows peaks at 414, 493, 619, 670, 1,008, and 1,135 cm^{-1}, differing greatly from the spectra collected on the green material which show Raman peaks at 1,106, 1,158 and 1,522 cm^{-1} (Figure 13C).

The results of laboratory Raman investigations performed on the measured types/samples described in the previous sections (Sections 3.1–3.5) are summarized in Table 2. In the Ravine of Fools site, we found abundant quartz associated with oxides (goethite) and sulfates (natrojarosite). The sample collected in Berrocal is characterized by a complex mineralogical association: augite, titanite, epidote, K-feldspar, and quartz are representative of the unaltered rock while natrojarosite and hematite are only found in the external crust of the sample. In the samples collected in the sites: Pequeño Grand Canyon and La casa de los Sordos we found

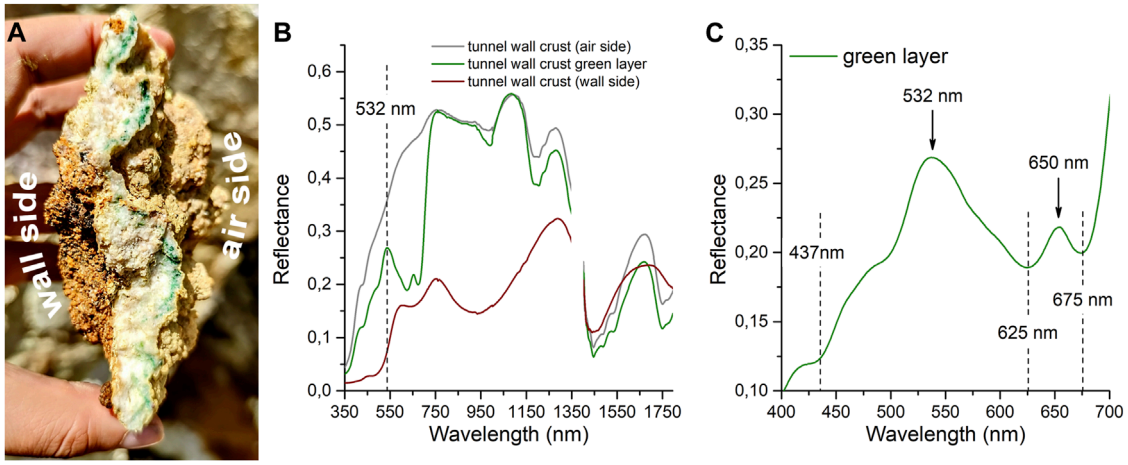

FIGURE 10
(A) Mineral crust sample collected from the left wall of the tunnel containing inside it a green layer of organic matter, the left side of the sample was the one attached to the wall; **(B)** Spectra collected on the wall side, on the green layer, and the white crust, the gap in the spectra is due to the removal of spectral range that is affected by large noise; **(C)** Spectrum of the green layer, the dashed lines highlight the main absorption bands and the arrows indicate the scattering peaks in the visible range.

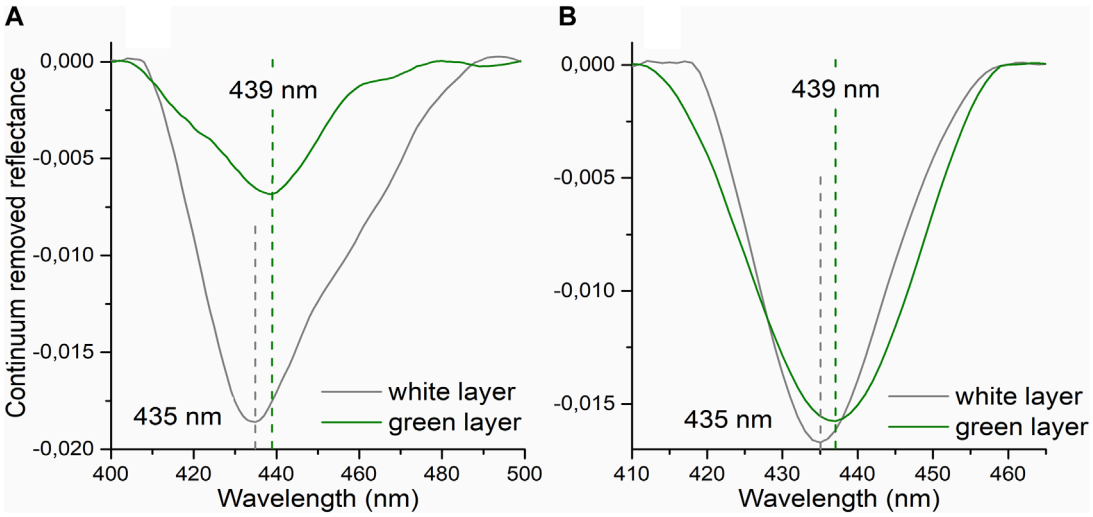

FIGURE 11
Continuum removed spectra of white mineral crust and green patina/layer. **(A)** spectra collected on the tunnel wall; **(B)** spectra collected outside the tunnel on the sample of Figure 8. The dashed lines indicate the band center position.

evidence of clay minerals (illite) in association with coquimbite, quartz, feldspar, barite, and hematite.

4 Discussion

The VIS-NIR measurement campaign in the Río Tinto area allowed us to collect a large dataset of spectra related to products resulting from acid alteration of the volcanic rock in place.

The data collected on the river terrace at the Ravine of Fools location show a great spectral variability that can be attributed to high mineralogical diversity. This diversity was found by probing a only few centimeters of sediment on a river terrace to simulate the acquisitions that the Ma_MISS spectrometer will perform in the Martian subsurface during the Rosalind Franklin rover mission.

In particular, the VIS-NIR data obtained on layers A, C, and E (e.g., Figure 4) show absorptions related to the presence of transition elements that generate charge transfer and crystal field effects carried out with absorption bands at about 500 and 650, and 900 nm. These bands specifically can be due to the presence of iron in both minerals such as oxides and sulfates. In fact, the presence of bands near 650 nm is typical of both sulfates and non-sulfates bearing ferric iron (Cloutis et al., 2006). In the case of the presence of sulfates, one of the discriminants is the presence of an absorption band at near 1,700–1,800 nm (Clark et al., 1990), which, in this case, cannot be relied on because of the lack of data in the visible part of the

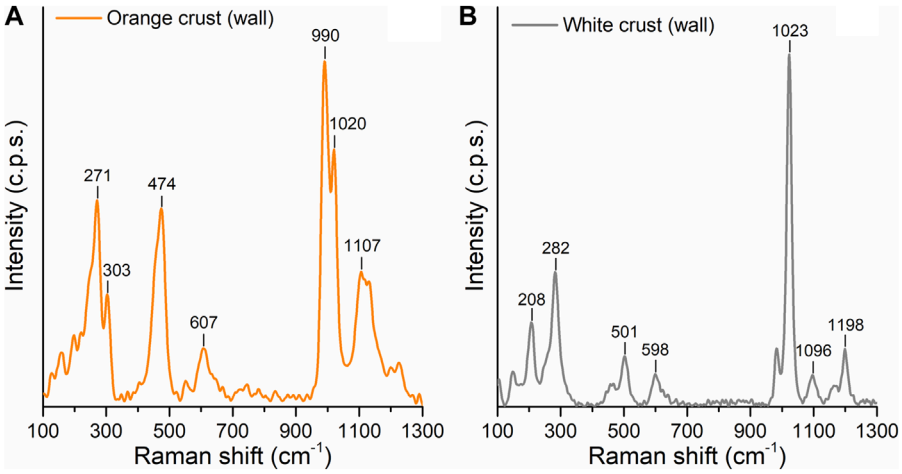

FIGURE 12
Laboratory micro-Raman spectra collected on tunnel wall minerals. **(A)** orange efflorescence; **(B)** white efflorescence.

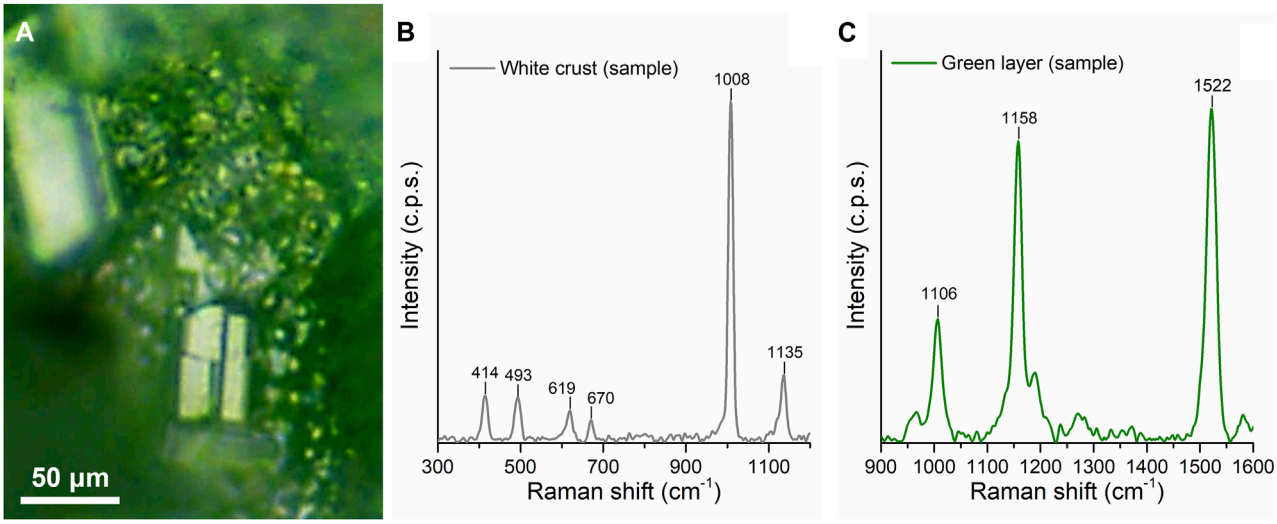

FIGURE 13
Micro-Raman analysis of the mineral crust sample collected in the tunnel (i.e., Figure 10A): **(A)** optical image (50x) of the green layer in the crust sample showing the colorless crystals and the green material; **(B)** Raman spectrum collected on white mineral crust; **(C)** Raman spectrum collected on the green material.

spectral range. A further discriminant between oxides and sulfates may be the presence of absorption bands in the spectral region near 2,200 nm (e.g., Figure 4A). Absorptions in this region, are not present in compositions of iron oxides while they were detected in the spectra of layers A, C, and E. In particular, the presence of a band centered at 2,200 nm could be attributed to Al-OH type bonds in clay minerals or aluminum-bearing sulfates such as alunite (Clark et al., 1990) whose presence might not be excluded in soils formed by acid alteration of aluminum-rich rocks (Mavris et al., 2018). Layers B and D show different spectra from each other. In the case of layer B, this appears to contain less iron than layer D, both because of the presence of shallower absorptions in the visible part of the range (i.e., CTA and CFA) and because layer D shows a deeper band at 2,265 nm that is usually detected in the spectra of ferric sulfates like jarosite (Cloutis et al., 2006). Layer B, on the other hand, shows absorption with two minima (2,165 and 2,210 nm) that are found in the spectra of kaolinite, a mineral that has been detected by techniques other than VIS-NIR spectroscopy in the Río Tinto area as an alteration product of feldspar bearing rocks (García-Palomero, 1980; Fernández-Remolar et al., 2011). Also in this layer, there is an absorption band at 2,265 nm that is shallower than that found in layer D related to the possible presence of jarosite. Within the stratigraphy examined at the Ravine of Fools locality, a black spot (i.e., F spectrum) was also measured, which appears substantially featureless with a marked red slope attributable to a coal-like composition. Contrary to the VIS-NIR data, the micro-Raman acquired on the Ravine of Fool samples show in the case of layers A, C, and E the presence of quartz crystal grains as remnants

TABLE 2 Result of Raman analysis performed on the collected samples.

Locations	Sample	Raman peaks (cm^{-1})	Assignements
Ravine of Fools	Layer A	462, 125	Quartz
	Layer B	1,010, 622, 437, 221, 137	Natrojarosite
		462, 125	Quartz
	Layer C	698, 465, 392, 302	Quartz + Goethite
	Layer D	N.D.	N.D.
	Layer E	458, 109	Quartz
Pequeño Grand Canyon	White layer	466, 203, 150	Illite + quartz
	Grey layer	150	Illite
		1,198, 1,098, 1,023, 601, 501, 280, 209, 143	Coquimbite
Berrocal	Red crust	394, 283, 219	Hematite
	Yellow crust	1,154, 1,103, 1,008, 625, 565, 436,296, 223, 137	Jarosite
	Unaltered rock	1,010, 828, 667, 552, 392, 357, 325, 191	Augite
		1,160, 807, 695, 610, 466, 395, 354, 262, 205, 128	Quartz
		1,088, 1,609, 513, 470, 280, 153	Calcite + K-feldpar
		911, 608, 536, 467, 316, 255, 176, 165, 145, 112	Titanite
		1,094, 1,048, 986, 912, 894, 881, 677, 606, 570, 461, 426, 395, 349, 275, 255, 204	Epidote
La casa de los Sordos	Grey sediment	466, 203, 150	Illite + quartz
	Purple sediment	605, 409, 290, 226	Hematite
		985, 616, 460	Barite
		464, 205, 127	Quartz
		507, 478, 457, 292, 183, 148	Albite
Tunnel	Orange efflorescence (wall)	1,107, 1,020, 990, 607, 474, 303, 271	Ferricopiapite
	White efflorescence (wall)	1,198, 1,096, 1,023, 598, 501, 282, 208	Coquimbite
	White mineral crust (sample)	1,135, 1,008, 679, 619, 493, 414	Gypsum
	Green layer (sample)	1,522, 1,158, 1,106	Carotenoids

of the metamorphosed volcanic rock. This is because quartz has no absorption features in the VIS-NIR range. In addition, was detected also goethite in layer C, in accordance with CTA and CFA spectral signatures (e.g., Figure 4B) In the case of layer B, Raman data show the presence of jarosite confirming the results obtained in the field (i.e., presence of 2,265 nm band).

The data obtained from the measurements collected in the stratigraphy of the mining tailing basin (i.e., the Pequeño Grand Canyon, Figure 6) essentially shows two compositions that appear spectrally different mainly regarding the depth of the bands rather than in terms of band center positions. The spectra of the two layers also show an absolute reflectance level that differs by 20%. The greater depth of the hydration bands near 1,400 and 1,900 nm in the gray layers than in the white layers is related to a greater presence in the former of coquimbite as detected in the Raman data. At the same time, our laboratory results show the presence of illite in both samples which is responsible for the 2,206 nm Al-OH absorption band. The greater depth of this band in the white layers can be explained by a higher abundance of illite which is characterized by a marked prominence of the band near 2,200 nm with respect to the 1,400 and 1,900 nm bands. Our results obtained in the Pequeno Grand Canyon confirm the results of Fernandez-Remolar et al. (2011) which detected the widespread presence of illite in the studied area.

In the Berrocal site, we detected the effect of the acidic aqueous alteration on a volcanic rock. In particular, the VIS-NIR spectrum

collected on the fresh side of the sample is dominated by the signatures related to the epidote (i.e., 2,257 and 2,350) as the results of the metamorphic process that characterized the volcanic rock of the area (Munhá, 1990). On the same side of the sample micro-Raman confirms the presence of epidote along with another metamorphic (i.e., titanite, calcite) and primary minerals (i.e., quartz, K-feldspar). In the altered external crusts, the VIS-NIR data detected two different acidic alteration products, namely, oxides and sulfates (i.e., blue, and red spectrum in Figure 7D respectively). The bands at 930, 680, and 500 nm suggest the presence of hematite as confirmed while the presence of the 2,265 nm absorption (i.e., red spectrum in Figure 7D) indicates the occurrence of jarosite as confirmed by the micro-Raman results.

The fluvial sediments measured in la Casa de los Sordos, show spectral features, in particular the absorptions near 880 and 550 nm that are consistent with Fe^{3+} oxides like hematite while the small absorption near 440 nm suggests the hydroxo-bridged Fe^{3+} that could be found in iron-bearing sulfates (Cloutis et al., 2006). The presence of sulfates like jarosite may be further indicated by the 2,265 nm absorption bands which are found in both spectra (e.g., Figure 8C). In addition, VIS-NIR spectra show the presence of the band at 2,206 nm which, as previously discussed, can be attributed to the presence of illite. Raman data complement the VIS-NIR results confirming the presence of illite in grey sediments and hematite, barite, quartz, and albite in the purple one.

On the tunnel walls, although with limitations related to low illumination (only the visible range was usable), spectroscopy revealed three different compositions (e.g., Figure 9). The spectrum collected on the orange efflorescence shows absorptions in the first part of the range (350–500 nm) and near 850 nm, these spectra characteristics are typical of sulfates and iron oxides spectra. Despite the different spectral shapes, the spectrum collected on the white efflorescence also shows features attributable to iron-bearing minerals (Cloutis et al., 2006). The study of the mineral crust sample collected from the wall (e.g., Figure 10) and measured outside the tunnel shows markedly different compositions between the side where it was attached to the wall and the side exposed to the air. The side attached to the wall shows a spectral shape and absorptions typical of goethite/hematite-type iron oxides (Ben-Dor et al., 2006). The white part of the mineral crust, which contains the green layer within it and that constitutes the exposed side of the sample, shows the typical three minima in the hydration-related bands resembling the spectrum of gypsum (Clark et al., 1990). Regarding the green patina found inside the tunnel, this shows spectral characteristics analog to that found on the green layer that lies inside the mineral crust sample detached from the tunnel walls. In both cases, the spectra collected on the green zone do not show a red slope in the visible range but show *Chl-a* absorption at 440 and 675 nm, a *phycocyanin* absorption at 620 nm, a fluorescence peak at 650 nm, and a scattering peak in the green region (532 nm) consistent with the literature regarding the cyanobacteria spectra (Gitelson et al., 1999; Kutser, 2004).

Raman measurements revealed that the mineralogy of the tunnel walls is dominated by iron sulfates (e.g., Figure 12). As has already been extensively documented, the precipitation sequence of the Río Tinto waters involves the formation of trivalent iron sulfates such as ferricopiapite and coquimbite (Rull et al., 2014; 2022). Raman spectra acquired on the sample collected on the tunnel wall confirmed that the mineral crust containing the green layer consists of gypsum crystals (e.g., Figure 13). In this case, the presence of gypsum can be attributed to the interaction between the cement mortar used to build the tunnel and low-pH sulfate solutions (Liu et al., 2015). The collected spectrum on the green layer shows Raman peaks at 1,522, 1,158, and 1,106 cm^{-1} which are commonly attributed to $\nu1$(C=C), $\nu2$(C-C) stretching mode, and δ(C-CH_3) bending mode of carotenoids (Jehlička, et al., 2014; Němečková, et al., 2022). Specifically, the Raman peak related to the $\nu1$(C=C) vibration at 1,522 cm^{-1} falls in the range of values found when in the presence of lutein, β-carotene, zeaxanthin, and astaxanthin (Jehlička, et al., 2014). This finding reinforces the observation that gypsum rocks can also support endolithic communities (Parnell et al., 2004; Dong et al., 2007).

The VIS-NIR spectral properties of the green, organic material under the orange and white efflorescences (e.g., Figure 9C) appear to be the same as that measured within the gypsum crust (e.g., Figure 10C). This confirms that different types of sulfates (Ca- and Fe-bearing) still allow the development of endolithic communities in close contact. In particular, gypsum and potentially other Fe-bearing sulfates can provide a microenvironment that protects these organisms from exposure to extreme temperatures, UV flux, and desiccation, yet they are translucent enough to allow for photosynthesis and nitrogen fixation in rock (Rothschild et al., 1994; Boison et al., 2004). In this case, however, we have not made determinations regarding the UV shielding capacity of the gypsum compared to the iron sulfates found in the tunnel, even if this aspect has been extensively studied (Gomez et al., 2003) with results that indicate the sulfates of iron have greater shielding capabilities against solar radiation (Martinez-Frias et al., 2006). However, this aspect remains relevant given the spread of sulfate deposits on Mars (Clark et al., 1982; Cooper and Mustard, 2002; Gendrin et al., 2005; Wang and Ling, 2011; Meslin et al., 2022) resulting in potential sites that could host Martian life.

Our laboratory VIS-NIR on-field and Raman measurements found typical mineralogies resulting from alteration processes in an acid environment. Our results are in full agreement with previous studies in the area that have defined the alteration pathways of the rocks that characterize the study area and described their resulting products (Fernandez-Remolar et al., 2005; Fernandez-Remolar et al., 2011). Although the presence of phyllosilicates and sulfates has also been found on Mars through data from orbiting missions and rover missions (Poulet et al., 2005; 2008; Wang et al., 2006; Bibring et al., 2007; Mustard et al., 2008; Carter et al., 2016; Mandon et al., 2021; Turner et al., 2021; Brossier et al., 2022) and although the origin of these minerals may be related to different processes and source mineralogies than those in the Río Tinto (Mangold et al., 2007; Bishop et al., 2008; Mandon et al., 2021), VIS-NIR spectroscopy has proven to be an important tool for characterizing the mineralogy of the studied area. The detection of organic matter capable of modifying the spectral shape both by introducing specific absorptions and scattering peaks in the spectrum (as in the case of the green material in the tunnel) and by introducing variations of the spectral slope (as in the case of featureless carbonaceous material found at the Ravine of fools) confirms that the VIS-NIR spectroscopy is a very sensitive tool for the detection of acid alteration products in geological samples considered as Martian analogs. This in turn highlights the

importance of VIS-NIR spectroscopy in monitoring the possible presence of biosignatures on the subsurface of Mars.

Especially, VIS-NIR data coupled with Raman data were even more effective. Our way of proceeding during this campaign was to simulate the synergies that will be put in place between some of the instruments onboard the next mission to Mars by the Rosalind Franklin rover. On the rover, the Ma_MISS spectrometer operating in the VIS-NIR will be able to make point measurements in the Martian subsurface at various depths, which may coincide with areas where the sample will be taken that will later be measured inside the Analytical Laboratory Drawer by the Raman spectrometer (RLS, Rull et al., 2017), and by the spectrometer operating in the NIR MicrOmega (Bibring et al., 2017).

5 Conclusion

In this work, we describe the standard procedures and the results followed during our geological field analysis campaign in the Río Tinto area. This geologically/biologically well-documented site with its rock/water/biology interaction represents an ideal open-air laboratory where to collect spectral data and samples useful for testing the Rosalind Franklin/Ma_MISS spectrometer. The scientific results obtained by this, and previous works made with other drilling equipment (Bonaccorsi and Stoker, 2008) and with other scientific instruments (Gomez et al., 2011) confirm that this type of activity in the Río Tinto area site is important for enriching the scientific community's grasp on the Martian environment and for obtaining key information on the mineralogical and geochemical evolution of the Martian surface/subsurface. The data collected on-field and in the laboratory were analyzed and compared to reconstruct the composition of the analyzed samples/sites.

We focused our efforts on any spectral signature related to the presence of biomarkers in the collected data since we know that the Ma_MISS instrument could aid in detecting organics (Ferrari et al., 2023) in the Martian subsoil, which is one of the main scientific objectives of the Rosalind Franklin rover mission.

Mineralogies found in the Río Tinto area through our investigations with VIS-NIR and Raman spectroscopy appear to be in full agreement with previous studies of the area which used different analytical techniques (García-Palomero, 1980; Fernandez-Remolar et al., 2011).

The detection of clays at some of the sites visited confirms that the Río Tinto can also be considered a good analogue of Martian environments such as Oxia Planum. Although in this case differently at Oxia Planum the aluminum-rich clays seem to be predominant.

This study also reaffirms that the synergy between VIS-NIR and Raman is an excellent combination both for mineralogical characterizations but also for biosignature detection in mineral matrices.

Furthermore, these activities on terrestrial analogs improve our understanding of life in extreme conditions and how it can be preserved in the form of biosignatures and detected by the scientific instruments that will be on board the next missions to Mars. The use of complementary techniques that have different sensitivities in detecting specific phases proved to be effective in the analysis of unknown geologic samples. The combination of these spectroscopic techniques adopted on the Rosalind Franklin Rover will be fundamental to the characterization of the Martian subsurface. For this reason, we believe that scientific activities carried out at terrestrial analog sites with instrumentation comparable to that used in space missions are of fundamental importance both to test the instrumentation and to build specific databases useful for the interpretation of scientific data. Thus, this work provides crucial preparation for the exploitation and interpretation of the scientific data that the Ma_MISS instrument will supply during the active phase of the mission. This activity is also useful for defining the priorities of the astrobiological objectives on the ground.

Data availability statement

The raw data supporting the conclusion of this article will be made available by the authors, without undue reservation.

Author contributions

MF coordinated the Río Tinto campaign, collected field and laboratory data, made data analyses, and wrote the manuscript. SD collected VIS-NIR measurements on the field. AF performed the geological survey of the visited area. EB collected micro-Raman spectra in the laboratory and participated in the writing of the manuscript. FG, who is an expert in the Río Tinto analog site, guided the group during the campaign for searching peculiar mineralogies and biosignatures. MD supervised the work as the PI of the Ma_MISS instrument. All authors contributed to the article and approved the submitted version.

Funding

This work is supported by the Italian Space Agency (ASI) grant ASI-INAF n. 2017-412-H.0. Ma_MISS is funded by ASI and INAF. Europlanet 2024 RI has received funding from the European Union's Horizon 2020 research and innovation programme under Grant Agreement No. 871149.

Conflict of interest

The authors declare that the research was conducted in the absence of any commercial or financial relationships that could be construed as a potential conflict of interest.

Publisher's note

References

Aguilera, A., Gómez, F., Lospitao, E., and Amils, R. (2006b). A molecular approach to the characterization of the eukaryotic communities of an extreme acidic environment: Methods for DNA extraction and denaturing gradient gel electrophoresis analysis. *Syst. Appl. Microbiol.* 29, 593–605. doi:10.1016/j.syapm.2006.01.006

Aguilera, A., Manrubia, S. C., Gómez, F., Rodríguez, N., and Amils, R. (2006a). Eukaryotic community distribution and its relationship to water physicochemical parameters in an extreme acidic environment, Río Tinto (southwestern Spain). *Appl. Environ. Microbiol.* 72, 5325–5330. doi:10.1128/AEM.00513-06

Aguilera, A., Souza-Egipsy, V., Gómez, F., and Amils, R. (2007). Development and structure of eukaryotic biofilms in an extreme acidic environment, Río Tinto (SW, Spain). *Microb. Ecol.* 53, 294–305. doi:10.1007/s00248-006-9092-2

Aguilera, A. (2013). Eukaryotic organisms in extreme acidic environments, the río tinto case. *Life*53 (3), 363–374. doi:10.3390/life3030363

Amaral Zettler, L. A., Gómez, F., Zettler, E., Keenan, B. G., Amils, R., and Sogin, M. L. (2002). Eukaryotic diversity in Spain's river of fire. *Nature* 417, 137. doi:10.1038/417137a

Amils, R., González-Toril, E., Fernández-Remolar, D., Gómez, F., Aguilera, Á., Rodríguez, N., et al. (2007). Extreme environments as Mars terrestrial analogs: The Rio Tinto case. *Space Sci.* 55, 370–381. doi:10.1016/j.pss.2006.02.006

Ben-Dor, E., Levin, N., Singer, A., Karnieli, A., Braun, O., and Kidron, G. J. (2006). Quantitative mapping of the soil rubification process on sand dunes using an airborne hyperspectral sensor. *Geoderma* 131, 1–21. doi:10.1016/j.geoderma.2005.02.011

Bibring, J. P., Arvidson, R. E., Gendrin, A., Gondet, B., Langevin, Y., Le Mouelic, S., et al. (2007). Coupled ferric oxides and sulfates on the Martian surface. *Science* 317 (5842), 1206–1210. doi:10.1126/science.1144174

Bibring, J. P., Hamm, V., Pilorget, C., Vago, J. L., and Team, M. (2017). The MicrOmega investigation onboard ExoMars. *Astrobiology* 17, 621–626. doi:10.1089/ast.2016.1642

Bigham, J. M., Schwertmann, U., Traina, S. J., Winland, R. L., and Wolf, M. (1996). Schwertmannite and the chemical modeling of iron in acid sulfate waters. *Geochimica Cosmochimica Acta*60 (12), 2111–2121. doi:10.1016/0016-7037(96)00091-9

Bishop, J. L., Dobrea, E. Z. N., McKeown, N. K., Parente, M., Ehlmann, B. L., Michalski, J. R., et al. (2008). Phyllosilicate diversity and past aqueous activity revealed at Mawrth Vallis, Mars. *Science* 321 (5890), 830–833. doi:10.1126/science.1159699

Boison, G., Mergel, A., Jolkver, H., and Bothe, H. (2004). Bacterial life and dinitrogen fixation at a gypsum rock. *Appl. Environ. Microbiol.* 70, 7070–7077. doi:10.1128/AEM.70.12.7070-7077.2004

Bonaccorsi, R., and Stoker, C. R. (2008). Science results from a mars drilling simulation (Río Tinto, Spain) and ground truth for remote science observations. *Astrobiology.* 8, 967–985. doi:10.1089/ast.2007.0152

Brossier, J., Altieri, F., De Sanctis, M. C., Frigeri, A., Ferrari, M., De Angelis, S., et al. (2022). Constraining the spectral behavior of the clay-bearing outcrops in Oxia Planum, the landing site for ExoMars "Rosalind Franklin" rover. *Icarus* 386, 115114. doi:10.1016/j.icarus.2022.115114

Carter, J., Quantin, C., Thollot, P., Loizeau, D., Ody, A., and Lozach, L. (2016). "Oxia Planum, a clay-laden landing site proposed for the ExoMars rover mission: Aqueous mineralogy and alteration scenarios," in 47th Lunar and Planetary Science Conference, Woodlands, Texas, March 21–25, 2016, 206. LPI Contribution No. 1903.

Christensen, P. R., Morris, R. V., Lane, M. D., Banfield, J. L., and Malin, M. C. (2001). Global mapping of martian hematite mineral deposits: Remnants of water-driven processes on early mars. *J. Geophys. Res.* 106, 23873–23885. doi:10.1029/2000JE001415

Ciarletti, V., Clifford, S., Plettemeier, D., Le Gall, A., Hervé, Y., Dorizon, S., et al. (2017). The WISDOM radar: Unveiling the subsurface beneath the ExoMars rover and identifying the best locations for drilling. *Astrobiology*17, 565–584. doi:10.1089/ast.2016.1532

Clark, B. C., Baird, A. K., Weldon, R. J., Tsusaki, D. M., Schnabel, L., and Candelaria, M. P. (1982). Chemical composition of Martian fines. *J. Geophys. Res.* 87 (B12), 10059–10067. doi:10.1029/JB087iB12p10059

Clark, R. N., King, T. V. V., Klejwa, M., Swayze, G. A., and Vergo, N. (1990). High spectral resolution reflectance spectroscopy of minerals. *J. Geophys. Res.* 95, 12653–12680. ISSN 0148-0227). doi:10.1029/JB095iB08p12653

Cloutis, E. A., Hawthorne, F. C., Mertzman, S. A., Krenn, K., Craig, M. A., Marcino, D., et al. (2006). Detection and discrimination of sulfate minerals using reflectance spectroscopy. *Icarus* 184, 121–157. doi:10.1016/j.icarus.2006.04.003

Coates, A. J., Jaumann, R., Griffiths, A. D., Leff, C. E., Schmitz, N., Josset, J.-L., et al. (2017). The PanCam instrument for the ExoMars rover. *Astrobiology*17, 511–541. doi:10.1089/ast.2016.1548

Cooper, C. D., and Mustard, J. F. (2002). Spectroscopy of loose and cemented sulfate-bearing soils: Implications for duricrust on mars. *Icarus* 158, 1. doi:10.1006/icar.2002.6874

De Angelis, S., De Sanctis, M. C., Ammannito, E., Carli, C., Di Iorio, T., Altieri, F., et al. (2014). The Ma_Miss instrument performance, I: Analysis of rocks powders by Martian VNIR spectrometer. *Planet. Space Sci.* 101, 89–107. doi:10.1016/j.pss.2014.06.010

De Angelis, S., Ferrari, M., De Sanctis, M. C., Altieri, A., Ammannito, E., Frigeri, A., et al. (2022). "The davis instrument: A new laboratory model for ExoMars 2022 Ma_MISS spectrometer," in 53rd LPSC (2022), Houston, Texas, OL, March 7–11, 2022. #1796.

De Sanctis, M. C., Altieri, F., Ammannito, E., Biondi, D., De Angelis, S., Meini, M., et al. (2017). Ma_MISS on ExoMars: Mineralogical characterization of the martian subsurface. *Astrobiology* 6-7, 612–620. doi:10.1089/ast.2016.1541

De Sanctis, M. C., Altieri, F., Ammannito, E., De Angelis, S., Ehlmann, B., Ferrari, M., et al. (2022). Exploring the shallow subsurface of mars with the Ma_MISS spectrometer on the ExoMars rover Rosalind Franklin. *Planet. Sci. J.* 3, 142. doi:10.3847/PSJ/ac694f

Dong, H., Rech, J. A., Jiang, H., Sun, H., and Buck, B. J. (2007). Endolithic cyanobacteria in soil gypsum: Occurrences in atacama (Chile), mojave (United States), and Al-jafr basin (Jordan) deserts. *J. Geophys. Res.* 112, G02030. doi:10.1029/2006JG000385

Farrand, W. H., Glotch, T. D., Rice, J. W., Hurowitz, J. A., and Swayze, G. (2009). Discovery of jarosite within the Mawrth Vallis region of Mars: Implications for the geologic history of the region. *Icarus* 204, 478–488. doi:10.1016/j.icarus.2009.07.014

Fernández-Remolar, D. C. (2003). Geological record of an acidic environment driven by iron hydrochemistry: The Tinto River system. *J. Geophys. Res.* 108, 5080. doi:10.1029/2002JE001918

Fernández-Remolar, D. C., Morris, R. V., Gruener, J. E., Amils, R., and Knoll, A. H. (2005). The Río Tinto Basin, Spain: Mineralogy, sedimentary geobiology, and implications for interpretation of outcrop rocks at Meridiani Planum, Mars. *Earth Planet. Sci. Lett.* 240, 149–167. doi:10.1016/j.epsl.2005.09.043

Fernández-Remolar, D. C., Prieto-Ballesteros, O., Gómez-Ortíz, D., Fernández-Sampedro, M., Sarrazin, P., Gailhanou, M., et al. (2011). Río Tinto sedimentary mineral assemblages: A terrestrial perspective that suggests some formation pathways of phyllosilicates on mars. *Icarus* 211, 114–138. doi:10.1016/j.icarus.2010.09.008

Ferrari, M., De Angelis, S., De Sanctis, M. C., Frigeri, A., Altieri, F., Ammannito, E., et al. (2023). Constraining the Rosalind Franklin rover/Ma_MISS instrument capability in the detection of organics. *Astrobiology* 23 (6), 691–704. doi:10.1089/ast.2022.0102

García-Palomero, F. (1980). *Caracteres geológicos y relaciones morfológicas y genéticas de los yacimientos del Anticlinal de Ríotinto, Huelva*. Padre Marchena: Instituto de Estudios Onubenses.

Gendrin, A., Mangold, N., Bibring, J. P., Langevin, Y., Gondet, B., Poulet, F., et al. (2005). Sulfates in martian layered terrains: The OMEGA/mars express view. *Science* 307, 1587–1591. doi:10.1126/science.1109087

Gitelson, A. A., Schalles, J. F., Rundquist, D. C., Schiebe, F. R., and Yacobi, Y. Z. (1999). Comparative reflectance properties of algal cultures with manipulated densities. *J. Appl. Phycol.* 11, 345–354. doi:10.1023/A:1008143902418

Goesmann, F., Brinckerhoff, W. B., Raulin, F., Goetz, W., Danell, R. M., Getty, S. A., et al. (2017). The mars organic molecule analyzer (MOMA) instrument: Characterization of organic material in martian sediments. *Astrobiology*17, 655–685. doi:10.1089/ast.2016.1551

Gomez, F., Grau, A., Vazquez, L., and Amils, R. (2003). "UV radiation effects over microorganisms and study of protective agents," in Proc. Of the III European Workshop on Exo-Astrobiology, Mars, The Search for Life, 18–20 November 2003, Madrid, Spain, 21–26.

Gomez, F., Walter, N., Amils, R., Rull, F., Klingelhöfer, A., Kviderova, J., et al. (2011). Multidisciplinary integrated field campaign to an acidic Martian Earth analogue with astrobiological interest: Rio Tinto. *Int. J. Astrobiol.* 10 (3), 291–305. doi:10.1017/S147355041100005X

Gómez, F., Rodriguez-Manfredi, J. A., Rodríguez, N., Fernández-Sampedros, M., Caballero-Castrejón, F. J., Amis, R., et al. (2012). Multidisciplinary integrated field campaign to an acidic Martian Earth analogue with astrobiological interest: Rio Tinto. *Int. J. Astrobiol.* 10 (3), 291–305. doi:10.1017/S147355041100005X

González-Toril, E., Llobet-Brossa, E., Casamayor, E. O., Amann, R., and Amils, R. (2003). Microbial ecology of an extreme acidic environment, the Tinto River. *Appl. Environ. Microbiol.* 69, 4853–4865. doi:10.1128/AEM.69.8.4853-4865.2003

Hughes, E. B., Gilmore, M. S., Martin, P. E., and Eleazer, M. (2023). Visible to near-infrared reflectance and Raman spectra of evaporites from sulfate-chloride Mars analogue brines. *Icarus* 401, 115597. doi:10.1016/j.icarus.2023.115597

Jehlička, J., Edwards, H. G. M., Osterrothová, K., Novotná, J., Nedbalová, L., Kopecký, J., et al. (2014). Potential and limits of Raman spectroscopy for carotenoid detection in microorganisms: Implications for astrobiology. *Phil. Trans. R. Soc.* 372, 20140199. doi:10.1098/rsta.2014.0199

Josset, J-L., Westall, F., Hofmann, B. A., Spray, J., Cockell, C., Kempe, S., et al. (2017). The close-up imager onboard the ESA ExoMars rover: Objectives, description, operations, and science validation activities. *Astrobiology*17, 595–611. doi:10.1089/ast.2016.1546

Korablev, O. I., Dobrolensky, Y., Evdokimova, N., Fedorova, A. A., Kuzmin, R. O., Mantsevich, S. N., et al. (2017). Infrared spectrometer for ExoMars: A mast-mounted instrument for the rover. *Astrobiology*17, 542–564. doi:10.1089/ast.2016.1543

Krzesinska, A., Bultel, B., Viennet, J.-C., Loizeau, D., and Werner, S. (2020). "Experimental approach to understand mineralogy and aqueous alteration history of Oxia Planum, ExoMars 2020 landing site," in EGU General Assembly 2020, Vienna, Austria, 4–8 May 2020, EGU2020–10649. doi:10.5194/egusphere-egu2020-10649

Kutser, Tiit (2004). Quantitative detection of chlorophyll in cyanobacterial blooms by satellite remote sensing. *Limnol. Oceanogr.* 6, 2179–2189. doi:10.4319/lo.2004.49.6.2179

Large, R. R., Gemmell, J. B., Paulick, H., and Huston, D. L. (2001). The alteration box plot: A simple approach to understanding the relationship between alteration mineralogy and lithogeochemistry associated with volcanic-hosted massive sulfide deposits. *Econ. Geol.* 96 (5), 957–971. doi:10.2113/96.5.957

Leblanc, M., Morales, J. A., Borrego, J., and Elbaz-Poulichet, F. (2000). 4,500-Year-old mining pollution in southwestern Spain: Long-term implications for modern mining pollution. *Econ. Geol.* 95, 655–662. doi:10.2113/gsecongeo.95.3.655

Leistel, J. M., Marcoux, E., Thiéblemont, D., Quesada, C., Sánchez, A., Almodóvar, G. R., et al. (1997). The volcanic-hosted massive sulphide deposits of the Iberian Pyrite Belt. *Min. Depos.* 33, 2–30. doi:10.1007/s001260050130

Liu, K., Deng, M., and Mo, L. (2015). Influence of pH on the formation of gypsum in cement materials during sulfate attack. *Adv. Cem. Res.* 27, 487–493. doi:10.1680/jadcr.14.00076

Mandon, L., Parkes Bowen, A., Quantin-Nataf, C., Bridges, J. C., Carter, J., Pan, L., et al. (2021). Morphological and spectral diversity of the clay-bearing unit at the ExoMars landing site Oxia Planum. *Astrobiology* 21, 464–480. doi:10.1089/ast.2020.2292

Mangold, N., Poulet, F., Mustard, J. F., Bibring, J.-P., Gondet, B., Langevin, Y., et al. (2007). Mineralogy of the nili fossae region with OMEGA/mars express data: 2. Aqueous alteration ofthe crust. *J. . Geophys. Res.*112, E08S04. doi:10.1029/2006JE002835

Martin-Izard, A., Arias, D., Arias, M., Gumiel, P., Sanderson, D. J., Castañon, C., et al. (2016). Ore deposit types and tectonic evolution of the Iberian Pyrite Belt: From transtensional basins and magmatism to transpression and inversion tectonics. *AstrobiologyOre Geology Reviews*79, 254–267. doi:10.1016/j.oregeorev.2016.05.011

Martinez-Frias, J., Amaral, G., and Vázquez, L. (2006). Astrobiological significance of minerals on Mars surface environment. *Rev. Environ. Sci. Biotechnol.* 5, 219–231. doi:10.1007/s11157-006-0008-x

Mavris, C., Cuadros, J., Nieto, J., Bishop, J., and Michalski, J. (2018). Diverse mineral assemblages of acidic alteration in the Rio Tinto area (southwest Spain): Implications for Mars. *Am. Mineralogist* 103 (12), 1877–1890. doi:10.2138/am-2018-6330

Meslin, P. -Y., Forni, O., Beck, P., Cousin, A., Beyssac, O., Lopez-Reyes, G., et al. (2022). "Evidence for perchlorate and sulfate salts in jezero crater, mars, from supercam observations," in 53rd Lunar and Planetary Science Conference, Woodlands, Texas, March 7–11, 2022.

Mitrofanov, I. G., Litvak, M. L., Nikiforov, S. Y., Jun, I., Bobrovnitsky, Y. I., Golovin, D. V., et al. (2017). The ADRON-RM instrument onboard the ExoMars rover. *Astrobiology*17, 585–594. doi:10.1089/ast.2016.1566

Munhá, J. (1990). "Metamorphic evolution of the south Portuguese/pulo do lobo zone," in *Pre-mesozoic evolution of iberia*. Editors R. D. Dallmeyer, and E. Martínez García (Berlin: Springer Verlag), 363–368.

Mustard, J., Murchie, S., Pelkey, S., Ehlmann, B. L., Milliken, R. E., Grant, J. A., et al. (2008). Hydrated silicate minerals on mars observed by the mars reconnaissance orbiter CRISM instrument. *Nature* 454, 305–309. doi:10.1038/nature07097

Nachon, M., Clegg, S. M., Mangold, N., Schröder, S., Kah, L. C., Dromart, G., et al. (2014). Calcium sulfate veins characterized by ChemCam/Curiosity at Gale crater, Mars. *J. Geophys. Res. Planets* 119, 1991–2016. doi:10.1002/2013JE004588

Němečková, K., Culka, A., and Jehlička, J. (2022). Detecting pigments from gypsum endoliths using Raman spectroscopy: From field prospection to laboratory studies. *J. Raman Spectrosc.* 53, 630–644. doi:10.1002/jrs.6144

Parnell, J., Lee, P., Cockell, C. S., and Osinski, G. R. (2004). Microbial colonization in impact-generated hydrothermal sulphate deposits, Haughton impact structure, and implications for sulphates on Mars. *Int. J. Astrobiol.* 3, 247–256. doi:10.1017/S1473550404001995

Poulet, F., Arvidson, R. E., Gomez, C., Morris, R. V., Bibring, J.-P., Langevin, Y., et al. (2008). Mineralogy of terra meridiani and Western arabia terra from OMEGA/MEx and implications for their formation. *Icarus* 195 (1), 106–130. doi:10.1016/j.icarus.2007.11.031

Poulet, F., Bibring, J.-P., Mustard, J. F., Gendrin, A., Mangold, N., Langevin, Y., et al. (2005). Phyllosilicates on Mars and implications for early martian climate. *Nature* 438 (7068), 623–627. doi:10.1038/nature04274

Quantin-Nataf, C., Carter, J., Mandon, L., Thollot, P., Balme, M., Volat, M., et al. (2021). Oxia Planum: The landing site for the ExoMars "Rosalind Franklin" rover mission: Geological context and prelanding interpretation. *Astrobiology* 21, 345–366. doi:10.1089/ast.2019.2191

Rieder, R., Gellert, R., Anderson, R. C., Brückner, J., Clark, B. C., Dreibus, G., et al. (2004). Chemistry of rocks and soils at Meridiani Planum from the alpha particle X-ray spectrometer. *Science* 306, 1746–1749. doi:10.1126/science.1104358

Rodríguez, N., Menéndez, N., Tornero, J., Amils, R., and De La Fuente, V. (2005). Internal iron biomineralization in imperata cylindrica, a perennial grass: Chemical composition, speciation and plant localization. *New Phytol.* 165, 781–789. doi:10.1111/j.1469-8137.2004.01264.x

Rossi, L., Ferrari, M., De Angelis, S., De Sanctis, M. C., Frigeri, A., Costa, N., et al. (2022). "A new laboratory model for Ma_MISS: The DAVIS setup and its laboratory drill," in 53rd LPSC (2022), Houston, Texas, OL, March 7–11, 2022. #1353.

Rothschild, L. J., Giver, L. J., White, M. R., and Mancinelli, R. L. (1994). Metabolic-activity of microorganisms in evaporites. *J. Phycol.* 30, 431–438. doi:10.1111/j.0022-3646.1994.00431.x

Rull, F., Veneranda, J. A., Manrique-Martinez, J. A., Sanz-Arranz, A., Saiz, J., Medina, J., et al. (2022). Spectroscopic study of terrestrial analogues to support rover missions to Mars – a Raman-centred review. *Anal. Chim. Acta* 1209, 339003. doi:10.1016/j.aca.2021.339003

Rull, F., Maurice, S., Hutchinson, I., Moral, A., Perez, C., Diaz, C., et al. (2017). The Raman laser spectrometer for the ExoMars rover mission to Mars. *Astrobiology* 17, 627–654. doi:10.1089/ast.2016.1567

Rull, F., Sobron, F., Guerrero Fernandez, J., Medina, J., Venegas, G., Gázquez, F., et al. (2014). "*In-situ* Raman analysis of the precipitation sequence of sulphate minerals using small droplets: Application to rio Tinto (Spain)," in *Mathematics of planet Earth. Lecture notes in Earth system Sciences*. Editors E. Pardo-Igúzquiza, C. Guardiola-Albert, J. Heredia, L. Moreno-Merino, J. Durán, and J. Vargas-Guzmán (Berlin, Heidelberg: Springer). doi:10.1007/978-3-642-32408-6_173

Schmidt, W. (2003). Iron solutions: Acquisition strategies and signaling pathways in plants. *Trends Plant Sci.* 8, 188–193. doi:10.1016/S1360-1385(03)00048-7

Squyres, S. W., Crotzinger, J. P., Arvidson, R. E., Bell, J. F., III, Calvin, W., Christensen, P. R., et al. (2004). *In situ* evidence for an ancient aqueous environment at meridiani Planum, mars. *Science* 306, 1709–1714. doi:10.1126/science.1104559

Turner, S. M. R., Schwenzer, S. P., Bridges, J. C., Rampe, E. B., Bedford, C. C., Achilles, C. N., et al. (2021). Early diagenesis at and below vera rubin ridge, Gale Crater, mars. *Meteorit. Planet Sci.* 56, 1905–1932. doi:10.1111/maps.13748

Vago, J. L., Westall, F., Coates, A. J., Jaumann, R., Korablev, O., Ciarletti, V., et al. (2017). Habitability on early mars and the search for biosignatures with the ExoMars rover. *Astrobiology* 17, 471–510. doi:10.1089/ast.2016.1533

Visviki, I., and Santikul, D. (2000). The pH tolerance of Chlamydomonas applanata (volvocales, Chlorophyta). *Arch. Environ. Contam. Toxicol.* 38, 147–151. doi:10.1007/s002449910018

Wang, A., Korotev, R. L., Jolliff, B. L., Haskin, L. A., Crumpler, L., Farrand, W. H., et al. (2006). Evidence of phyllosilicates in wooly patch, an altered rock encountered at west spur, columbia hills, by the spirit rover in gusev crater, mars. *J. Geophys. Res.* 111 (E2), E02S16. doi:10.1029/2005JE002516

Wang, A., and Ling, Z. C. (2011). Ferric sulfates on mars: A combined mission data analysis of salty soils at gusev crater and laboratory experimental investigations. *J. Geophys. Res.* 116, E00F17. doi:10.1029/2010JE003665

Zolotov, M., and Shock, E. (2005). Formation of jarosite-bearing deposits through aqueous oxidation of pyrite at Meridiani Planum, Mars. *Geophys. Res. Lett.* 32, L21203. doi:10.1029/2005GL024253